

## A green method for the synthesis of indeno[1,2-*b*]pyridines using Fe<sub>3</sub>O<sub>4</sub>@SiO<sub>2</sub>@PrSO<sub>3</sub>H as a nanomagnetic catalyst

Zohreh Kheilkordi<sup>a</sup>, Ghodsi Mohammadi Ziarani<sup>a,\*</sup>, Alireza Badiei<sup>b</sup>, Hossein Vojoudi<sup>b</sup>

<sup>a</sup>Department of Chemistry, Alzahra University, Vanak Square, P.O. Box 1993893973, Tehran, Iran.

<sup>b</sup>School of Chemistry, College of Science, University of Tehran, Tehran, Iran.

Received 20 April 2019; received in revised form 25 October 2019; accepted 26 November 2019

### ABSTRACT

The acidic agent (SO<sub>3</sub>H) was stabilized on the silica coated Fe<sub>3</sub>O<sub>4</sub> magnetic nanoparticles to produce Fe<sub>3</sub>O<sub>4</sub>@SiO<sub>2</sub>@Pr-SO<sub>3</sub>H, as a heterogeneous acidic catalyst, was designed, and then fully studied and characterized by FT-IR, XRD, TGA, DTA, TEM, and SEM analysis. Subsequently, the catalytic activity of Fe<sub>3</sub>O<sub>4</sub>@SiO<sub>2</sub>@PrSO<sub>3</sub>H was investigated by the one-pot four- component condensation reaction between 1,3-indandione, aromatic aldehydes, acetophenone or propiophenone and ammonium acetate under the solvent-free condition at 80 °C. The main advantages of this magnetic and heterogeneous acidic catalyst are high product yields, being environmentally benign, short reaction times, and easily separated from the reaction mixture using an external magnet.

**Keywords:** Fe<sub>3</sub>O<sub>4</sub>@SiO<sub>2</sub>@PrSO<sub>3</sub>H, Nanomagnetic heterogeneous catalyst, Indeno[1,2-*b*]pyridines, Multi component reaction, Solvent-free condition.

### 1. Introduction

Iron oxide nanoparticles can be characterized into four types: magnetite (Fe<sub>3</sub>O<sub>4</sub>), Maghemite (γ-Fe<sub>2</sub>O<sub>3</sub>), hematite (α-Fe<sub>2</sub>O<sub>3</sub>), Goethite (α-FeOOH) [1]. Among all the studied iron oxide nanoparticles, magnetite (Fe<sub>3</sub>O<sub>4</sub>) is one of the most popular materials in biotechnology, biomedical, analytical and biochemistry [2-6]. Therefore, up to now, various chemical methods have been used for the synthesis of magnetic nanoparticles including microemulsions [7], co-precipitation [8], sol-gel [9], sonochemical [10], hydrothermal [11], hydrolysis [12] and thermolysis of precursors [13]. Recently, there has been increasing attention in the application of magnetic nanoparticles as a catalyst in organic reactions due to their significant advantages, including reusability, high-surface-area, ease of recovery, ease of handling and economical [14-16]. The Surface of magnetic nanoparticles (MNPs) can be easily modified with organic and inorganic materials, which have been widely applied as a catalyst. Compounds containing pyridine groups are known in the broad

spectrum of biological activities such as anti-malarial [17], anesthetics [18], antiepileptics and anticonvulsants [19]. In continuation of our previous research in the field of heterogeneous catalysis [20-27], herein, we investigated the application of Fe<sub>3</sub>O<sub>4</sub>@SiO<sub>2</sub>@Pr-SO<sub>3</sub>H as in the synthesis of indeno[1,2-*b*]pyridines derivatives.

### 2. Experimental

All materials and methods were presented in the supporting information. The synthesis methods of nanoparticles including Fe<sub>3</sub>O<sub>4</sub> and Fe<sub>3</sub>O<sub>4</sub>@SiO<sub>2</sub> have been reported in the literature [28] and the supporting information of this article.

#### 2.1. Synthesis of sulfonic functionalized SiO<sub>2</sub> coated Fe<sub>3</sub>O<sub>4</sub> magnetic nanoparticles (Fe<sub>3</sub>O<sub>4</sub>@SiO<sub>2</sub>PrSO<sub>3</sub>H)

Modification of the prepared mesoporous magnetic materials with (3-mercaptopropyl) trimethoxysilane was performed as follows: 1 g SCMNPs was dispersed in 200 mL dried toluene, and then 25 mL of (3-Mercaptopropyl) trimethoxysilane in toluene (10% V/V) was added to above mixture under dry nitrogen atmosphere and refluxed for 24 h. The solid

\*Corresponding author.

Email: gmohammadi@alzahra.ac.ir (G. Mohammadi Ziarani)

product was magnetically gathered, washed with ethanol, and dried in vacuum. Then, the S-H group was converted to the SO<sub>3</sub>H group by a H<sub>2</sub>O<sub>2</sub>/MeOH (70/30 wt %) solvent mixture. The reaction mixture was stirred at room temperature for 12 h, followed by heating at 95 °C for 36 h. In the end, the Fe<sub>3</sub>O<sub>4</sub>@SiO<sub>2</sub>@PrSO<sub>3</sub>H nanoparticles were separated using an external magnet, washed with ethanol and H<sub>2</sub>O and dried at room temperature for 10 h.

## 2.2. General procedure for the synthesis of indeno [1,2-*b*]pyridine derivatives

A mixture of aromatic aldehydes (1 mmol), acetophenone or propiophenone (1 mmol), 1,3-indanedione (1 mmol, 0.14 gr), ammonium acetate (1.5 mmol, 0.11 gr) and Fe<sub>3</sub>O<sub>4</sub>@SiO<sub>2</sub>@PrSO<sub>3</sub>H (10 mol%, 0.01 gr) as a nanomagnetic heterogeneous catalyst was stirred under solvent free conditions at 80 °C for the suitable time defined in Table 2. The reaction progress was monitored using TLC (8:2, n-hexane/ethyl acetate). After completion of the reaction, the mixture was cooled to room temperature. Afterwards, hot ethanol was added to the reaction vessel, and the heterogeneous catalyst was separated using an external magnet. Finally, the solution was cooled to obtain a pure crystalline product. The new compound was characterized by IR, <sup>1</sup>H NMR, <sup>13</sup>C NMR and Mass spectroscopy techniques. The melting points and IR spectroscopy of the products were compared with those reported in the literature.

## Spectral data for new compound

### 4-(4-methoxyphenyl)-2-(4-bromophenyl)-indeno[1,2-*b*]pyridin-5-one (5i):

Yellow crystalline solid. FT-IR (KBr):  $\bar{\nu}$  = 3072, 1706, 1602, 1575, 1546, 1517, 1468, 1363 cm<sup>-1</sup>. <sup>1</sup>H NMR (500 MHz, DMSO):  $\delta$  = 3.86 (s, 3H, OMe), 7.06-7.08 (d, 2H, *J* = 8.4, Ar), 7.55 (t, 1H, *J* = 7.4 Hz, Ar), 7.66 (d, *J* = 7.3 Hz, 1H), 7.54-7.78 (m, 5H, Ar), 7.87 (s, 1H, Ar), 7.94-7.96 (d, *J* = 7.7 Hz, 1H, Ar), 8.27-8.29 (d, *J* = 8.6, 2.0 Hz, 2H, Ar) ppm. <sup>13</sup>C NMR (125 MHz, DMSO):  $\delta$  = 55.85,

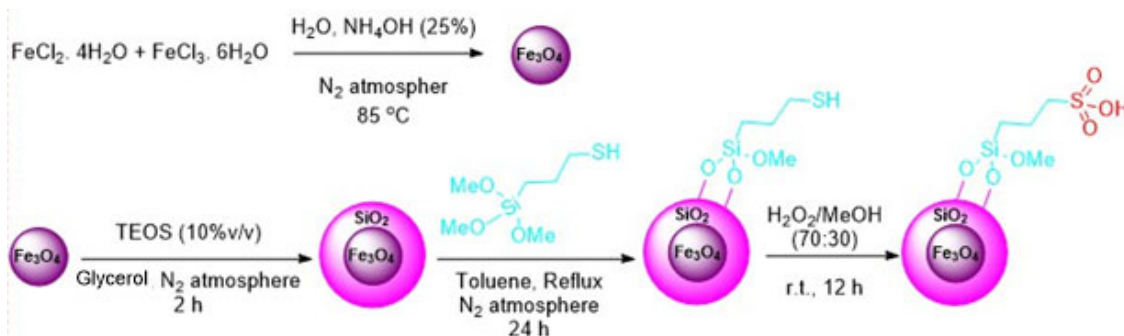
113.90, 121.18, 122.64, 123.95, 124.47, 127.28, 127.31, 129.84, 131.62, 131.93, 132.24, 135.39, 135.75, 137.16, 142.48, 149.34, 158.95, 161.10, 166.15, 190.66 ppm. Mass: (m/z) = 443 (M<sup>+</sup>), 426, 410, 390, 362, 345, 319, 290, 263, 243, 214, 187, 144, 102, 75.

## 3. Results and Discussion

### 3.1. Synthesis and characterization of Fe<sub>3</sub>O<sub>4</sub>@SiO<sub>2</sub>@PrSO<sub>3</sub>H

Fe<sub>3</sub>O<sub>4</sub>@SiO<sub>2</sub>@PrSO<sub>3</sub>H was synthesized according to the method shown in Scheme 1. At First, Fe<sub>3</sub>O<sub>4</sub> nanoparticles were synthesized through the reaction of FeCl<sub>2</sub>.4H<sub>2</sub>O and FeCl<sub>3</sub>.6H<sub>2</sub>O. Subsequently, a silica coating was laid on the Fe<sub>3</sub>O<sub>4</sub> NPs surfaces. After this, (3-mercaptopropyl) trimethoxysilane solution was reacted with SiO<sub>2</sub> coated Fe<sub>3</sub>O<sub>4</sub> magnetic nanoparticles (SCMNPs). Finally, Fe<sub>3</sub>O<sub>4</sub>@SiO<sub>2</sub>@PrSO<sub>3</sub>H was prepared by the oxidation of S-H group in the presence of H<sub>2</sub>O<sub>2</sub>/MeOH (70/30 wt %) solvent mixture (Scheme 1).

The structure of Fe<sub>3</sub>O<sub>4</sub>@SiO<sub>2</sub>@PrSO<sub>3</sub>H as a heterogeneous acidic catalyst was investigated and wholly characterized by FT-IR, XRD, TGA, DTA, SEM and TEM analysis. The FT-IR spectra of Fe<sub>3</sub>O<sub>4</sub>, Fe<sub>3</sub>O<sub>4</sub>@SiO<sub>2</sub> and Fe<sub>3</sub>O<sub>4</sub>@SiO<sub>2</sub>@PrSO<sub>3</sub>H were shown in Fig. 1. The spectrum of pure Fe<sub>3</sub>O<sub>4</sub> shows the strong absorption peaks at 573 and 457 cm<sup>-1</sup> for the stretching vibration of the Fe-O bonds. The absorption peaks of the coated silica on the Fe<sub>3</sub>O<sub>4</sub> at 1095 and 805 cm<sup>-1</sup> attributed to asymmetric stretching vibrations of Si-O-Si and stretching vibration of Si-O-H, respectively. The bending vibration of the Fe-O bonds observed in 1637 cm<sup>-1</sup>. Also, the absorption band at 3475 cm<sup>-1</sup> correspond to the hydroxyl bond in the SO<sub>3</sub>H group. The weak absorption band at 737 cm<sup>-1</sup> is attributed to the stretching vibration of the C-S group in the spectrum of Fe<sub>3</sub>O<sub>4</sub>@SiO<sub>2</sub>@PrSO<sub>3</sub>H. Finally, the absorption bands at 2970 and 2853 cm<sup>-1</sup> are related to the C-H stretch of the methylene group in the alkyl chain.



Scheme 1. Synthesis of Fe<sub>3</sub>O<sub>4</sub>@SiO<sub>2</sub>@PrSO<sub>3</sub>H nanoparticles.

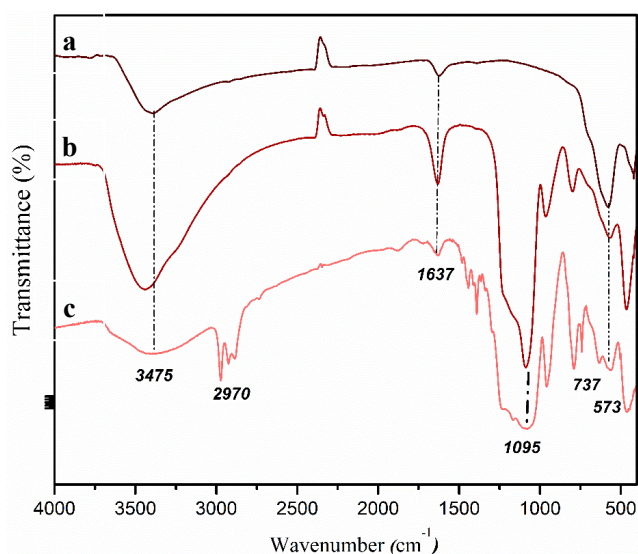


**Fig. 1.** FT-IR spectra of a) Fe<sub>3</sub>O<sub>4</sub>, b) Fe<sub>3</sub>O<sub>4</sub>@SiO<sub>2</sub>, and c) Fe<sub>3</sub>O<sub>4</sub>@SiO<sub>2</sub>@PrSO<sub>3</sub>H nanoparticles.

The XRD pattern of the synthesized Fe<sub>3</sub>O<sub>4</sub> and Fe<sub>3</sub>O<sub>4</sub>@SiO<sub>2</sub>@PrSO<sub>3</sub>H nanospheres was displayed in Fig. 2. The diffraction peaks at  $2\theta = 30.3^\circ, 35.7^\circ, 43.2^\circ, 53.3^\circ, 57.1^\circ,$  and  $62.5^\circ$  are corresponded to (220), (311), (400), (422), (511) and (440) planes, respectively, that It shows the presence of the magnetite phase with cubic spinals, a highly crystalline structure.

The curves of thermogravimetric analysis (TGA) and (DTA) for Fe<sub>3</sub>O<sub>4</sub>@SiO<sub>2</sub>@PrSO<sub>3</sub>H nanoparticles are shown in Fig. 3. The TGA curve of Fe<sub>3</sub>O<sub>4</sub>@SiO<sub>2</sub>@PrSO<sub>3</sub>H was shown the continuous weight loss of approximately 13% below 200 °C which can be attributed to the loss of adsorbed solvent or trapped water from the catalyst.

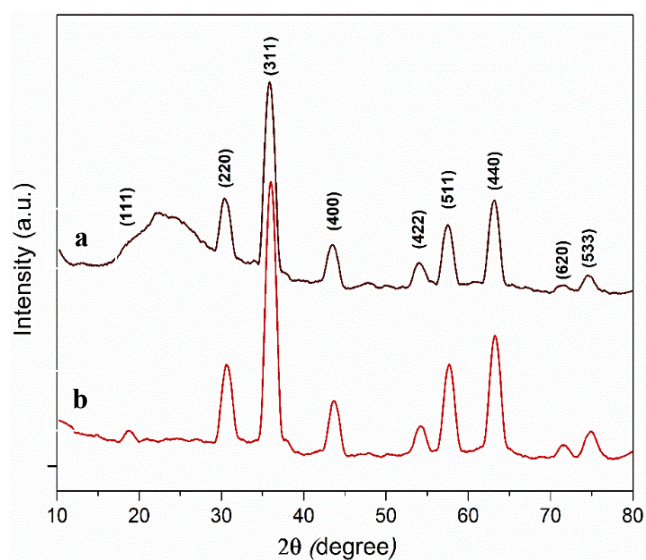


**Fig. 2.** X-ray diffraction patterns of a) Fe<sub>3</sub>O<sub>4</sub>, b) Fe<sub>3</sub>O<sub>4</sub>@SiO<sub>2</sub>@PrSO<sub>3</sub>H nanoparticles.

The weight loss of 21 % at 200 to 600 °C is related to the thermal decomposition of the organic functional groups in the Fe<sub>3</sub>O<sub>4</sub>@SiO<sub>2</sub>@PrSO<sub>3</sub>H nanoparticles, and the 2% weight loss at above 700 °C is affiliated to the self-condensation of the silanol groups. Also, the amount of the grafted organic compound was estimated to be about 0.03 mmol g<sup>-1</sup>. Further, the DTA peak has an endothermic and an exothermic signal, which is related to the evaporation of the water and the decomposition of organic compounds respectively. These results indicate that Fe<sub>3</sub>O<sub>4</sub>@SiO<sub>2</sub>@PrSO<sub>3</sub>H nanoparticles were successfully prepared (Fig. 3).

SEM images were showed the most of the nanoparticles have a uniform size with a spherical shape, and the diameter of Fe<sub>3</sub>O<sub>4</sub>@SiO<sub>2</sub>@PrSO<sub>3</sub>H is about 25-35 nm (Fig. 4). The TEM results show that the modified nanoparticles have a core-shell structure. The dark core represents the magnetic Fe<sub>3</sub>O<sub>4</sub>, and the lighter shell relate to the silica. In this analysis, the particle size was similar to SEM images.

### 3.2. Application of Fe<sub>3</sub>O<sub>4</sub>@SiO<sub>2</sub>@PrSO<sub>3</sub>H as MNPs catalyst in the synthesis of indeno[1,2-b]pyridine derivatives

Initially, for optimizing the reaction conditions, the four-component condensation of 4-cholorobenzaldehyde (1 mmol), 4-methoxyacetophenone (1 mmol), 1,3-indanedione (1 mmol, 0.14 gr), ammonium acetate (1.5 mmol) in the presence of Fe<sub>3</sub>O<sub>4</sub>@SiO<sub>2</sub>@PrSO<sub>3</sub>H (10 mol %, 0.01 gr) as a heterogeneous magnetic catalyst in various conditions as a reaction model were studied (Scheme 2).

Several conditions were investigated, including different solvents and the solvent-free conditions in different temperatures in the presence of Fe<sub>3</sub>O<sub>4</sub>@SiO<sub>2</sub>@PrSO<sub>3</sub>H, and also the catalyst-free condition (Table 1, entry 5). As shown results in Table 1, the solvent-free condition in the presence of Fe<sub>3</sub>O<sub>4</sub>@SiO<sub>2</sub>@PrSO<sub>3</sub>H at 80 °C was the best one.

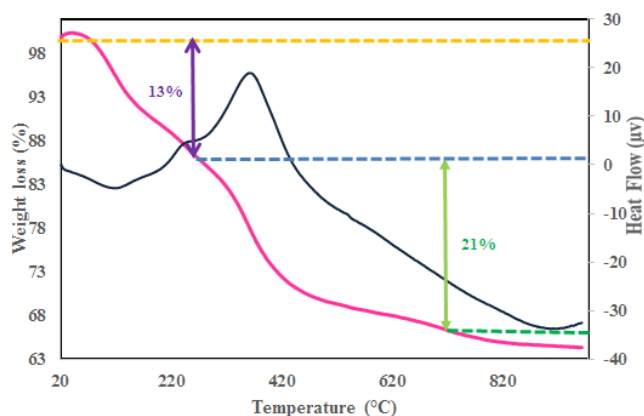


**Fig. 3.** TGA/DTA analysis of Fe<sub>3</sub>O<sub>4</sub>@SiO<sub>2</sub>@PrSO<sub>3</sub>H.

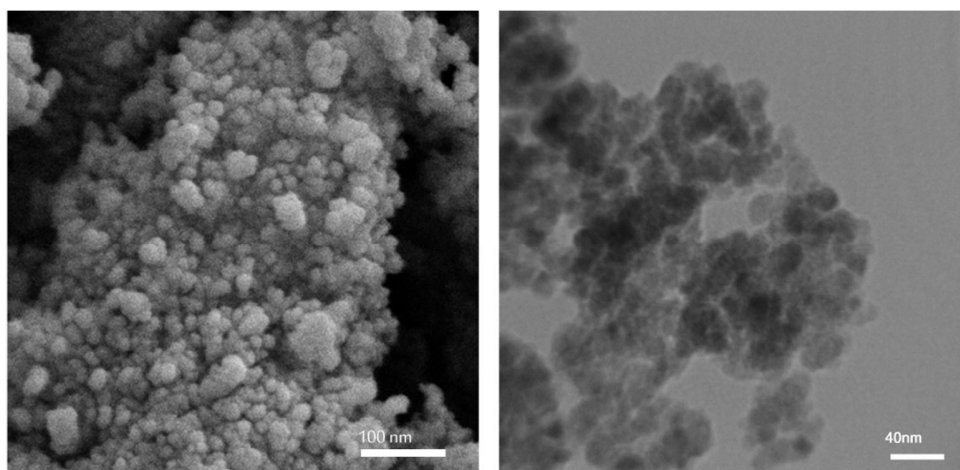
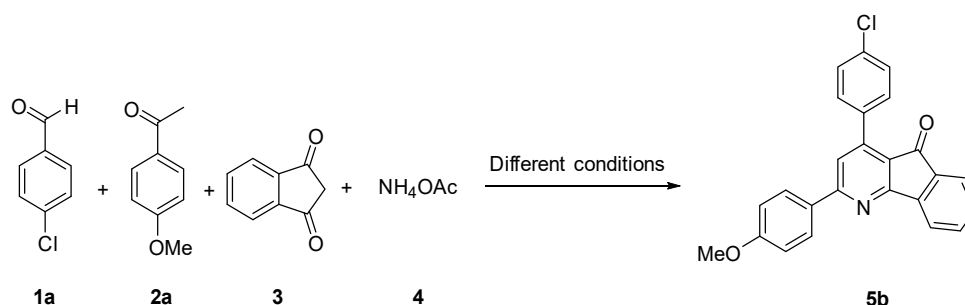


Fig. 4. SEM (left) and TEM (right) images of SCMNP-S magnetic nanomaterials.



Scheme 2. Synthesis of indeno[1,2-*b*]pyridine **5b** under different conditions.

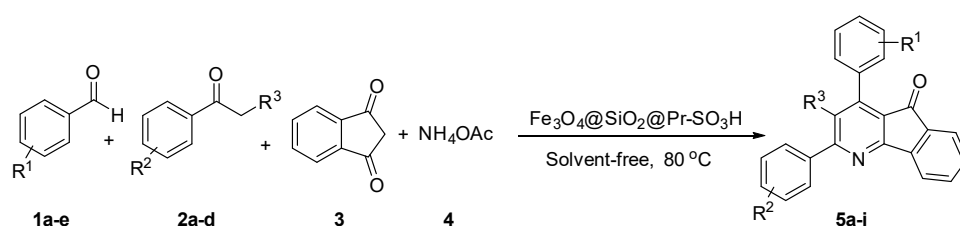
Table 1. Optimization of the reaction conditions in the synthesis of indeno[1,2-*b*]pyridine **5b**.

Entry	Catalyst	Solvent	Temp. (°C)	Time (h)	Yield (%) <sup>a</sup>
1	Fe <sub>3</sub> O <sub>4</sub> @SiO <sub>2</sub> @PrSO <sub>3</sub> H	H <sub>2</sub> O	Reflux	3	85
2	Fe <sub>3</sub> O <sub>4</sub> @SiO <sub>2</sub> @PrSO <sub>3</sub> H	EtOH	Reflux	2.5	86
3	Fe <sub>3</sub> O <sub>4</sub> @SiO <sub>2</sub> @PrSO <sub>3</sub> H	H <sub>2</sub> O:EtOH	Reflux	1.5	89
4	Fe <sub>3</sub> O <sub>4</sub> @SiO <sub>2</sub> @PrSO <sub>3</sub> H	-	80 °C	5 min	98
5	-	-	80 °C	12	45

<sup>a</sup>Isolated yields.

Then, the optimized reaction condition was applied to create a variety of indeno[1,2-*b*]pyridines from a range of aldehydes, 1,3-indandione, propiophenone or acetophenone derivatives and ammonium acetate using Fe<sub>3</sub>O<sub>4</sub>@SiO<sub>2</sub>@PrSO<sub>3</sub>H as an acidic catalyst in the solvent-free condition at 80 °C (Scheme 3)

and the new compound characterized by FT-IR, <sup>13</sup>C NMR, <sup>1</sup>H NMR and Mass spectra. As shown in Table 2, the reaction time for the electron deficient groups in the aromatic aldehydes was rather faster than that of electron donating groups.



Scheme 3. Synthesis of indeno[1,2-*b*]pyridine derivatives in the presence of Fe<sub>3</sub>O<sub>4</sub>@SiO<sub>2</sub>@PrSO<sub>3</sub>H.

**Table 2.** Synthesis of indeno[1,2-*b*]pyridine derivatives in the presence of Fe<sub>3</sub>O<sub>4</sub>@SiO<sub>2</sub>@PrSO<sub>3</sub>H (10 mol%) under the solvent-free conditions at 80 °C.

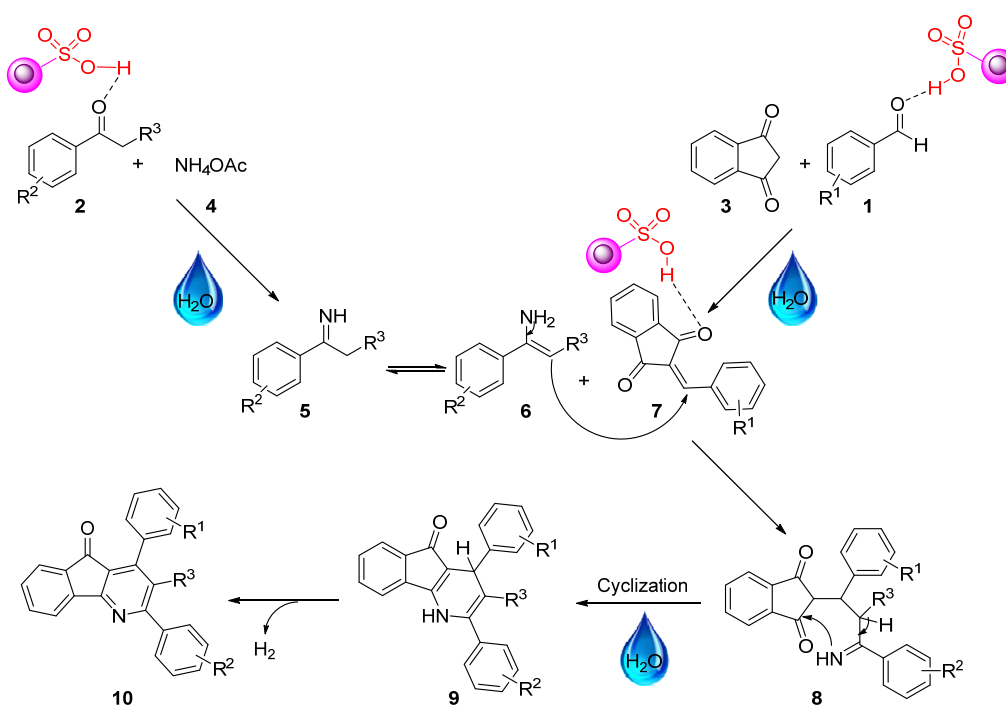
Entry	No.	R <sup>1</sup>	R <sup>2</sup>	R <sup>3</sup>	Time (min)	Yield (%)	m.p. (°C)		Ref.
							Found	Reported	
1	<b>5a</b>	4-Cl	H	H	5	95	197-199	186-188	[29]
2	<b>5b</b>	4-Cl	4-OMe	H	5	98	198-200	201-203	[30]
3	<b>5c</b>	4-Br	4-OMe	H	10	93	215-217	215-217	[30]
4	<b>5d</b>	3-NO <sub>2</sub>	4-OMe	H	10	92	223-225	220-222	[29]
5	<b>5e</b>	4-Me	4-OMe	H	18	90	166-169	160-161	[30]
6	<b>5f</b>	4-OMe	4-OMe	H	15	90	221-223	218-220	[30]
7	<b>5g</b>	4-Cl	H	Me	10	88	217-220	222-225	[31]
8	<b>5h</b>	3-NO <sub>2</sub>	H	Me	10	87	206-209	204-205	[30]
9	<b>5i</b>	4-OMe	Br	H	10	92	183-185	New	This work

The mechanism of this reaction was shown in (Scheme 4), as nano-Fe<sub>3</sub>O<sub>4</sub>@SiO<sub>2</sub>@PrSO<sub>3</sub>H activates both the carbonyl groups of the aromatic aldehyde **1** and acetophenone or propiophenone **2** as the electrophile species. The intermediate (enamine) **6** was prepared *via* the nucleophilic reaction of ammonium acetate **4** to the acetophenone or propiophenone compound, and also the intermediate **7** was produced by Knoevenagel condensation of aromatic aldehyde **4** with 1,3-indandione **3**. Then, the Michael addition between intermediate (enamine) **6** and intermediate **7** gave the

intermediate **8**, which followed by the cyclization and aromatization process to afford the final product **10**.

Finally, This green method improved the synthesis of indeno[1,2-*b*]pyridine derivatives in the different terms, including the reaction time and yield in comparing with the given data in the literature, as shown in Table 3.

The reusability and the recovery of the nanomagnetic catalyst were determined for the preparation of compound **5b** for three runs under the optimized reaction conditions as shown in Table 4, and the yield of each run was 96, 93, and 89 %, respectively.

**Scheme 4.** A suggested mechanism for the synthesis of indeno[1,2-*b*]pyridine derivatives.

**Table 3.** Comparison of different conditions in the synthesis of compound **5b**.

Entry	Catalyst	Solvent	Conditions	Time (h)	Yield (%)	Ref.
1	-	DMF	MW, 120 °C	8 min	85	[29]
2	Cu-ZnO	EtOH/H <sub>2</sub> O	r.t.	1.5	95	[30]
3	-	THF	80 °C	2	88	[31]
4	Fe <sub>3</sub> O <sub>4</sub> @SiO <sub>2</sub> @PrSO <sub>3</sub> H	-	80 °C	5 min	96	This work

**Table 4.** Reusability of the Fe<sub>3</sub>O<sub>4</sub>@SiO<sub>2</sub>@PrSO<sub>3</sub>H

Entry	Time (min)	Yield (%)
1	5	96
2	5	93
3	7	89

#### 4. Conclusions

In conclusion, the synthesis of indeno[1,2-*b*]pyridine derivatives were developed in the presence of nano-Fe<sub>3</sub>O<sub>4</sub>@SiO<sub>2</sub>@PrSO<sub>3</sub>H as a heterogeneous catalyst under green conditions. This method had several advantages such as simple and inexpensive work up procedure, eco-friendly, short reaction time, high yield, and reusability of the nano-Fe<sub>3</sub>O<sub>4</sub>@SiO<sub>2</sub>@PrSO<sub>3</sub>H catalyst.

#### Acknowledgements

The authors thank the financial support from the Research Council of Alzahra University and the University of Tehran.

#### References

- [1] R.M. Cornell, U. Schwertmann, The iron oxides: structure, properties, reactions, occurrences and uses, John Wiley & Sons, 2003.
- [2] M. Amiri, M. Salavati-Niasari, A. Pardakhty, M. Ahmadi, A. Akbari, Mater. Sci. Eng. C. 76 (2017) 1085-1093.
- [3] H. Khojasteh, M. Salavati-Niasari, M.-P. Mazhari, M. Hamadani, RSC Adv. 6 (2016) 78043-78052.
- [4] M. Amiri, M. Salavati-Niasari, A. Akbari, Microchim. Acta. 184 (2017) 825-833.
- [5] M. Wierucka, M. Biziuk, TrAC, Trends Anal. Chem. 59 (2014) 50-58.
- [6] M. R. Shishehbore, A. Afkhami, H. Bagheri, Chem. Cent. J. 5 (2011) 1-10.
- [7] M. Darbandi, F. Stromberg, J. Landers, N. Reckers, B. Sanyal, W. Keune, H. Wende, J. Phys. D: Appl. Phys. 45 (2012) 1-11.
- [8] C. Blanco-Andujar, D. Ortega, Q. A. Pankhurst, N. T. K. Thanh, J. Mater. Chem. 22 (2012) 12498-12506.
- [9] N. Ahmed, M. Michelin-Jamois, H. Fessi, A. Elaissari, Soft Matter. 8 (2012) 2554-2564.
- [10] C. S. Ciobanu, S. L. Iconaru, E. Gyorgy, M. Radu, M. Costache, A. Dinischiotu, P. Le Coustumer, K. Lafdi, D. Predoi, Chem. Cent. J. 6 (2012) 1-12.
- [11] H. Bae, T. Ahmad, I. Rhee, Y. Chang, S.-U. Jin, S. Hong, Nanoscale Res. Lett. 7 (2012) 1-5.
- [12] X. Wang, J. Zhou, C. Miao, Y. Wang, H. Wang, C. Ma, S. Sun, J. Nanopart. Res. 14 (2012) 1-7.
- [13] P. Guardia, N. Pérez, A. Labarta, X. Batlle, Langmuir, 26 (2009) 5843-5847.
- [14] C. O. Dalaigh, S. A. Corr, Y.G. Ko, S. J. Connon, Angew. Chem. 46 (2007) 4329-4332.
- [15] F. Shi, M. K. Tse, M. M. Pohl, A. Bruckner, S. Zhang, M. Beller, Angew. Chem. Int. Ed. 46 (2007) 8866-8868.
- [16] D. H. Zhang, G. D. Li, J. X. Li, J. S. Chen, Chem. Commun. 29 (2008) 3414-3416.
- [17] B. Y. Kim, J. B. Ahn, H. W. Lee, S. K. Kang, J. H. Lee, J. S. Shin, S. K. Ahn, C. I. Hong, S. S. Yoon, Eur. J. Med. Chem. 39 (2004) 433-447.
- [18] P. K. Tapaswi, C. Mukhopadhyay, Arkivoc, (x) (2011) 287-298.
- [19] S. Matsumoto, N. Miyamoto, T. Hirayama, H. Oki, K. Okada, M. Tawada, H. Iwata, K. Nakamura, S. Yamasaki, H. Miki, Bioorg. Med. Chem. 21 (2013) 7686-7898.
- [20] G. Mohammadi Ziarani, Z. Kazemi Asl, P. Gholamzadeh, A. Badiei, M. Afshar, Appl. Organomet. Chem. 31 (2017) 1-7.
- [21] G. Mohammadi Ziarani, Z. Kazemi Asl, P. Gholamzadeh, A. Badiei, M. Afshar, J. Sol-Gel Sci. Technol. 85 (2018) 103-109.
- [22] V. Fathi Vavsari, G. Mohammadi Ziarani, S. Balalaie, A. Latifi, M. Karimi, A. Badiei, Tetrahedron, 72 (2016) 5420-5426.
- [23] G. Mohammadi Ziarani, Z. Kazemi Asl, P. Gholamzadeh, A. Badiei, M. Afshar, Inorg. Nano-Met Chem. 48 (2018) 1-6.
- [24] T. Ahmadi, G. Mohammadi Ziarani, S. Bahar, A. Badiei, J Iran Chem Soc. 15 (2018) 1153-1161.
- [25] Z. Kheilkordi, G. Mohammadi Ziarani, S. Bahar, A. Badiei, J Iran Chem Soc. 16 (2019). 365-372.
- [26] G. Mohammadi Ziarani, A. Badiei, S. Mousavi, N. Lashgari, A. Shahbazi, Chin J Catal. 33 (2012) 1832-1839.
- [27] Z. Kheilkordi, G. Mohammadi Ziarani, N. Lashgari, A. Badiei, Polyhedron. 166 (2019) 203-209
- [28] A. Banaei, H. Vojoudi, S. Karimi, S. Bahar, E. Pourbasheer, RSC Adv. 5 (2015) 83304-83313.
- [29] S. Tu, B. Jiang, R. Jia, J. Zhang, Y. Zhang, Tetrahedron Lett. 48 (2007) 1369-1374.
- [30] H. Alinezhad, S. M. Tavakkoli, P. Biparva, Chin. J. Catal. 35 (2014) 560-564.
- [31] M. Daryabari, S. Khaksar, J. Mol. Liq. 198 (2014) 263-266.